Atmos. Chem. Phys. Discuss., 10, 16475–16496, 2010
www.atmos-chem-phys-discuss.net/10/16475/2010/
doi:10.5194/acpd-10-16475-2010

Atmospheric Chemistry and Physics Discussions

Deep convective clouds at the tropopause

H. H. Aumann[1] **and S. G. DeSouza-Machado**[2]

[1]California Institute of Technology, Jet Propulsion Laboratory, CA, USA
[2]Department of Physics, University of Maryland, Baltimore County, Baltimore, MD, USA

Received: 24 April 2010 – Accepted: 28 May 2010 – Published: 2 July 2010

Correspondence to: H. H. Aumann (aumann@jpl.nasa.gov)

Published by Copernicus Publications on behalf of the European Geosciences Union.

Abstract

Data from the Advanced Infrared Sounder (AIRS) on the EOS Aqua spacecraft identify thousands of cloud tops colder than 225 K, loosely referred to as Deep Convective Clouds (DCC). Many of these cloud tops have "inverted" spectra, i.e. areas of strong water vapor, CO_2 and ozone opacity, normally seen in absorption, are now seen in emission. We refer to these inverted spectra as DCCi. They are found in about 0.4% of all spectra from the tropical oceans excluding the Western Tropical Pacific (WTP), 1.1% in the WTP. The cold clouds are the anvils capping thunderstorms and consist of optically thick cirrus ice clouds. The precipitation rate associated with DCCi suggests that imbedded in these clouds, protruding above them, and not spatially resolved by the AIRS 15 km FOV, are even colder bubbles, where strong convection pushes clouds to within 5 hPa of the pressure level of the tropopause cold point. Associated with DCCi is a local upward displacement of the tropopause, a cold "bulge", which can be seen directly in the brightness temperatures of AIRS and AMSU channels with weighting function peaking between 40 and 2 hPa, without the need for a formal temperature retrieval. The bulge is not resolved by the analysis in numerical weather prediction models. The locally cold cloud tops relative to the analysis give the appearance (in the sense of an "illusion") of clouds overshooting the tropopause and penetrating into the stratosphere. Based on a simple model of optically thick cirrus clouds, the spectral inversions seen in the AIRS data do not require these clouds to penetrate into the stratosphere. However, the contents of the cold bulge may be left in the lower stratosphere as soon as the strong convection subsides. The heavy precipitation and the distortion of the temperature structure near the tropopause indicate that DCCi are associated with intense storms. Significant long-term trends in the statistical properties of DCCi could be interesting indicators of climate change.

ACPD

10, 16475–16496, 2010

1 Introduction

Inspection of Advanced Infrared Sounder (AIRS, Aumann et al., 2003) spectra shows the expected absorption features of water, carbon dioxide and ozone relative to spectral regions of low atmospheric opacity (window areas) in almost all spectra, including those with heavy cloud cover. However, for about 1% of the spectra in the tropics (30 S–30 N) the spectra are inverted: the strong CO_2 absorption near 14 µm, the strong water vapor absorption near 6 µm and ozone absorption in the 10 µm area are seen in emission relative to cold cloud top in atmospheric window channels. Negative brightness temperature differences between the 11 µm window and 6.7 µm water channel were first noted by Ackerman (1996). Schmetz et al. (1997) noted their association with severe thunderstorms and first attributed it to Overshooting Convection (OC). Conceptually, OC forces water vapor into the lower stratosphere where it emits at the warmer stratospheric temperature. Romps and Kuang (2009) defined overshooting cloud tops as clouds with brightness temperature colder than the monthly tropopause temperature climatology at that location, as derived from the NCEP reanalysis (Kalnay et al., 1996). Others have used the reanalysis pertaining to the time and location of the observation to infer a number of reference levels. The relatively coarse temporal, spatial and vertical resolution of the reanalysis make the accuracy of the calculated height of the tropopause uncertain (Liu and Zipser, 2005), particularly in the presence of strong convection. What appears as OC and penetration into the stratosphere, may actually be related to the difference between the height of the tropopause under average conditions and strong convection conditions. The objective of our paper is to use AIRS hyperspectral data to gain new insights into properties of these cold cloud tops.

The utility of using the inversion of strong atmospheric absorption lines for the definition of the tropopause in the presence of deep convection relies on having a large and reasonably predictable amount of absorption above and below the tropopause. Strong CO_2 or water lines could be used, but not ozone lines, since there is relatively little ozone below the tropopause. The spectral inversion was first noted in the water vapor

ACPD
10, 16475–16496, 2010

sensitive 6.7 µm channel of the MeteoSat sounder. Here we use the AIRS 1419 cm^{-1} channel. Under tropical clear conditions the weighting function of this channel, due to water vapor absorption, peaks near 200 hPa. Depending on the details of the temperature and water vapor profile, the brightness temperature measured at 1419 cm^{-1}, bt1419, is 65 to 85 K colder than the brightness temperature in the 1231 cm^{-1} atmospheric window channel, bt1231. However, water vapor absorption poses a potential problem, since bt1419 is a function of temperature and water vapor mixing ratio in the atmospheric column. Observations that strong convection "moistens" the upper troposphere (Ray and Rosenlof, 2007) and speculations that strong convection may result in injection of water vapor into the stratosphere complicate the interpretation of inverted water vapor spectra. For this reason we use CO_2 absorption. The weighting function of the strong CO_2 line near 712 cm^{-1} also peaks near 200 hPa, but this peak is almost independent of the water vapor profile. The difference between window channels at 961 cm^{-1} and 790 cm^{-1} (bt961 and bt790) channels provides additional insight into the cloud optical depth and the location of the cloud top relative to the tropopause.

2 Data

We use the data from AIRS, supported by data from the Advanced Microwave Sounder Unit (AMSU, Lambrigtsen et al., 2003) and the Advanced Microwave Scanning Radiometer for EOS (AMSRE, Imaoka et al., 2007). AIRS, AMSU and AMSRE were launched in May 2002 on the EOS Aqua satellite in to a 705 km altitude sun-synchronous, 98 degree inclination circular orbit. The 1:30 p.m. ascending node, in the following referred to as the "day" overpass, and a corresponding 1:30 a.m. "night" overpass on the descending part of each orbit are actively maintained. The orbit period is 98.99 min and, since the orbit is sun-synchronous, consecutive orbits are separated by 2760 km at the equator. More than seven years of AIRS, AMSU and AMSRE data are now available.

ACPD
10, 16475–16496, 2010

AIRS is a hyperspectral infrared sounder which covers the 650 to 2665 cm^{-1} region of the thermal infrared spectrum with 2378 spectral channels. The AIRS footprint subtends an angle of 1.1 degree (full width 1/2 peak), corresponding to a 15 km footprint at nadir. The footprints are scanned ±49.5 degrees cross-track, resulting in a 1650 km wide swath with 90 footprints. The absolute calibration at the 200 mK level and stability at the better than 10 mK/year level have been validated using the sea surface temperatures (Aumann et al., 2006). The validation of the radiometric accuracy and stability at the extremely cold temperatures relevant for the study of cold cloud tops used Dome Concordia data in Antarctica (Walden et al., 2006; Elliott et al., 2007). AMSU is a microwave radiometer with 14 channels centered on the 57 GHz oxygen line with a 3.3 degree (full width at 1/2 peak), which is synchronized with AIRS and covers the same crosstrack swath. AMSRE is a conical scanning passive microwave imaging radiometer. The rain rates, measured within minutes of the AIRS data, are available each day averaged on a 0.25 degree grid, i.e., approximately on a 28 km scale. Data from AIRS and AMSU since September 2002 are available from the GDIS at GSFC. The AMSRE rain rates (Wilheit et al., 2003) were obtained from ftp://rain.atmos.colostate.edu/RAINMAP/data/amsre/. Unlike AIRS and AMSU data, which are calibrated radiances and brightness temperatures (level 1b), the AMSRE rain rates are based on a level 3 (gridded data) product.

Data for our study were collected in three sets. This allows us to contrast clear, random, and extremely cloudy conditions. For the first set we identified each day typically 30 000 cloud-free spectra. In the second set we collected typically 20 000 random spectra, selected within one degree of nadir, regardless of land/ocean or cloud status. For the third set we collected all objects with brightness temperatures colder than 225 K in the 1231 cm^{-1} atmospheric window channel between latitude 40 S and 40 N. We refer to these objects as Deep Convective Clouds (DCC). This set typically consisted of 15 000 spectra each day. For the evaluation of spectral properties and comparison with the model calculations we used a number of AIRS channels, including 712 cm^{-1}, 790 cm^{-1}, 961 cm^{-1}, 1231 cm^{-1} and 1419 cm^{-1}. We refer to the

ACPD
10, 16475–16496, 2010

brightness temperatures measured in these channels as bt712, bt790, etc. and define DW=bt1231−bt1419, DT=bt1231−bt712, and DC=bt961−bt790. The measurements at these cold temperatures require very high instrument sensitivity. The Noise equivalent Delta Temperature (NeDT) is a measure of the uncertainty in the brightness temperature in a single measurement. It is commonly quoted at 280 K. For example for the 1231 cm^{-1} channel, NeDT280=0.05 K; however for a much colder scene, NeDT200=0.31 K. The effective noise for difference measurements is further amplified, e.g. stdev(DT) is close to 0.5 K.

2.1 Spectral characterization

Figure 1a shows the DCC for the night tropical oceans as a scatter diagram of DT vs. bt1231 from the night overpasses from 6 September 2010. The red line is the scatter diagram ridge line. This line highlights the most likely functional dependence of the two variables in the scatter diagram. It is generated by dividing the x-axis into equal width bins and connecting the mean value of each bin (red circles). Figure 1b shows the scatter diagram derived from simulations, which will be described in Sect. 3. The difference between two window channels which straddle the 11 µm window, DC, contains additional information to characterize the cloud. Figure 2a shows a scatter diagram of DC vs. DT for the same data as Fig. 1a. Figure 2b shows the corresponding scatter diagram derived from the simulations.

2.2 Frequency of DCC

The data base created by the random nadir spectra was used to calculate mean properties of cold clouds for various thresholds. The frequency of occurrence is defined as the number of spectra which pass a threshold divided by the total number of spectra in a given area, expressed as percent. There are large regional differences between the Western Tropical Pacific (WTP) and tropical ocean (TO) exclusive of the WTP. We also

ACPD
10, 16475–16496, 2010

separated day (1:30 p.m. local time overpass) and night (1:30 a.m. local time overpasses). Results are summarized in Table 1.

2.3 Temperature structure related to DCC

In the presence of high cloud overcast conditions it is difficult to measure the temperature structure near the tropopause in the thermal IR or with 57 GHz microwave channels. However, we can use AIRS and AMSU temperature sounding channels to evaluate the lapse rate in the lower stratosphere to infer conditions near the tropopause. The 668.2 cm^{-1} (bt668) and 679.9 cm^{-1} (bt679) AIRS channels measure the brightness temperature in broad layers near 2 and 40 hPa, respectively. Figure 3a shows the scatter diagram of the temperature at 2 hPa and 40 hPa as function of bt1231 from the 6 September 2006. Only the scatter diagram ridge lines are shown. As bt1231 becomes colder than 210 K the temperature at 2 hPa gets warmer, while the temperature at 40 hPa gets colder. Since bt679 at 40 hPa may be effected by the presence of clouds, we checked with AMSU data, which are much less effected by clouds than IR channels. There are no exact equivalent channels, but AMSU#14 and AMSU#9 measure the temperature in broad layers near 2 and 60 hPa, respectively. Figure 3b shows an overlay of the scatter diagrams of AMSU#14-AMSU#9 and bt669-bt679.9. Only the scatter diagram ridge lines are shown. The 7 year mean temperature at 60 hPa (AMSU#9) under DT< −2 K conditions is 1.7 K colder during the day, 2.4 K colder at night than under random conditions. The temperature at 2 hPa (AMSU#14) is 0.1 K warmer for the day time observations, 1.7 K warmer for the night time observations under DT< −2 K conditions than under random conditions. Table 2 summarizes various parameters for 7 years of AIRS/AMSU and AMSRE observations for the tropical oceans, separating day and night, and the WTP from the remaining tropical ocean (TO), under random conditions and for DCC identified by inverted spectra with DT< −2 K.

ACPD
10, 16475–16496, 2010

2.4 Rain rate

We use the rain rate measured by AMSRE to evaluate the correlation between rain rate and DCC. Since AMSRE and AIRS are on the same spacecraft, the DCC identification with AIRS and the rain rates measured with AMSRE daily gridded product are time coincident within minutes. The measurements are not exactly simultaneous because AIRS is cross-track scanning within 0.1 degree of nadir, while AMSRE uses a forward looking conical scan. Figure 4 is a scatter diagram of the rain rate as function of DT. There is large scatter, but the ridge lines show the rapid increase in the rain rate for DT<0 K, and even faster at DT< −2 K. Since the AMSRE rain rate refers to the average in a 28 km grid, the rain rate in the 15 km AIRS FOV could be considerably larger. Table 2 includes the rain rate.

3 Simulations

The observed brightness temperatures allow a physical interpretation of the height of the cloud tops relative to the height of the tropopause. We used model calculations for 34 tropical ocean profiles from a combination of two data sets: the set of regression profiles (including the AFGL profiles) used by Strow et al. (2003) to make the AIRS Fast Model Radiative Transfer Algorithm (RTA), and the TIGR3 (1999) data base. The chosen profiles had mean tropopause pressure 100 hPa, range 56 to 125 hPa, mean cold point temperature 195 K, range 185 K to 207 K. The tropopause was defined by the coldest point in the profiles. The profiles were selected to cover the dynamic range of likely tropical ocean profiles (surface temperature and column water amount greater than or equal to [299.7 K, 41 mm] corresponding to the AFGL Tropical Profile), not their distribution. For each model profile we simulated the spectra for optically thick cirrus clouds, with the effective particle sizes of the clouds being 20, 30 and 50 microns. Iwasaki et al. (2010) used 30 micron particles. For each of the three particle sizes used, the cloud top pressure was increased in 20 hPa steps from 120 hPa below to 60 hPa

ACPD
10, 16475–16496, 2010

above the tropopause pressure, but no models were used with cloud top pressure less than 30 hPa. The amount of cirrus ice was distributed in the RTA per the layer average pressure. The scattering part of the RTA used the Parametrization of Cloud Longwave Scattering for Atmospheric Modeling (PCLSAM) algorithm by Chou et al. (1999). Ice aggregate scattering parameters were based on Baran (2003). The integrated Ice Water Content (IWC) of 5 g/m^3 was selected to approximate the mean observed DC under DT< −2 K conditions. This number is larger than that determined by Iwasaki et al. (2010), as they studied the sub visible cirrus blown off the top of a DCC cloud, while in this paper we are more interested in studying the overall characteristics of optically thick DCC. The cloud bottom pressure in the model was always 150 hPa larger than the cloud top pressure. This assumption is not critical since the clouds become optically thick within 20 hPa of the cloud top in all cases.

Figure 1b shows the results of the model calculation DT vs. bt1231 while Fig. 2b shows DC vs. DT. In both cases the calculations use 30 micron particles. Model spectra for 77 cloud tops more than 5 hPa above, 30 within 5 hPa of, and 204 more than 5 hPa below the tropopause are shown in blue (x), red (+), and green (o), respectively. Results from the same model calculations shown as function of bt1419 instead of bt712 look almost identical. The models with 20 and 50 micron effective particle sizes also look very similar. With 20, 30, and 50 micron effective sizes bt961−bt790 for cloud tops below the tropopause (green) increases from 1.6 K to 2.0 K to 2.5 K, but the clear separation between the blue, red and green cloud tops is unchanged.

4 Discussion

4.1 Model spectra and observation comparison

The label “Deep Convection” has been given to a wide range of objects identified by various thresholds, from cloud tops colder than 235 K, to 1 × 1 degree areas where the rain rate exceeds 1.6 mm/hr (Zelinka and Hartmann, 2009). The optical depth of

ACPD
10, 16475–16496, 2010

the clouds associated with deep convection is wavelength dependant and, since the clouds are likely to by spatially inhomogeneous, the label is sensitive to the size of the FOV. Table 1 shows that 3% of the spectra from the tropical oceans, almost 7% in the WTP, are identified as DCC based on bt1231<225 K. Most of the DCC with cloud tops between 210 K and 225 K in the tropical oceans are far below the tropopause. In the TO 0.8% of the spectra are inverted (DT<0 K or DW<0 K), 0.4% are identified with DT< −2 K or DW< −2 K. DDC which satisfy the DT< −2 K condition, referred to in the following as DCCi, reach very close to the tropopause. The near equivalence of DT and DW seen in the model calculations, is also seen in the observations summarized in Table 1. The table also allow a comparison with other work, although this is complicated by differences in the FOV used for other observations and possible calibration effects at cold temperatures. In the following we use CO_2 absorption to sense the height of the temperature inversion, which define as the height of the tropopause. The issue of possible water vapor enhancement above or below this inversion in the presence of DCC will be dealt with in another paper.

Figures 1b and 2b show that the DT< −2 K threshold fairly cleanly separates the cloud tops more than 5 hPa below the tropopause from the higher clouds. The additional DC>0.5 K test separates the clouds more than 5 hPa above (blue) from those more than 5 hPa below the tropopause (green). For the nominal tropical tropopause at 100 hPa, 5 hPa corresponds to 0.4 km altitude difference. The clear separation between cloud tops above and below the tropopause is provided by the window channel difference DC=bt961−bt790: the opacity of the ice clouds at 790 cm^{-1} is larger than the opacity at 961 cm^{-1}, i.e. the weighting function of the 790 cm^{-1} channel penetrates into the cloud for a small distance before the cloud become optically thick. If the cloud top is below the tropopause, bt790 is colder than bt961, i.e. DC>0 K, if the cloud top is above the tropopause then DC<0 K.

The comparison of Fig. 1a and b shows similarities in the slope as function of bt1231. However, the observations come to a sharp point at bt1231=180 K, DT=−12 K, while the blunt tip of the scatter diagram for the models is filled with cloud tops near and above

ACPD
10, 16475–16496, 2010

the tropopause. This indicates that the observations contain few cloud tops more than 5 hPa above the tropopause. This is confirmed in the comparison of the data in Fig. 2a and the model in Fig. 2b: Very few of the observed cloud tops have DC<0. The mean DC for clouds which satisfy the (DT< −2) conditions is +1 K with standard deviation of 0.65 K (Table 2), but is close to 2 K for lower cloud tops. The noise in DC due to detector noise alone is 0.5 K, i.e. the few observations with DC<0 are consistent with random noise. Figures 1b and 2b show model calculation using 30 micron effective particle size. For lower (warmer) cloud tops (0<DT<5 K) the models show little change in DC (DC=+2 K), while the observations show a gradient (from DC=1.5 K to DC=2 K). We attribute this difference to the simplification of using a fixed IWC, particle size and ice crystal habit for all models, including clouds well below the tropopause. Particle sizes are expected to diminish with height, as well as change structure.

4.2 Penetrating convection

The observation of inverted spectra has been taken as evidence of Overshooting Convection (OC, e.g. Schmetz et al., 1997), with the implication of tropopause penetration (Wang, 2007). The model calculations show that the inversion of spectra starts with cloud tops well below the tropopause. Figure 3 shows that the temperature structure near the tropopause in the presence of DCCi is distorted. The gradient between 2 and 40 hPa is 0.3 to 2 K steeper under DCCi conditions than at bt1231>225 K and warmer conditions. The steeper lapse rate means an unusually cold tropopause. This cold (upward) bulge in the tropopause causes the cloud top to be colder than, i.e. appear to overshoot, the temperature of the tropopause cold point derived from the analysis or reanalysis. However, water vapor, cirrus ice and pollutants collected in bulges may be left in the lower stratosphere, as soon as the strong convection subsides and the bulges disappear. This is consistent with observations of transport of pollutants into the lower stratosphere in the presence of strong convection, e.g. Randel et al. (2010).

There is evidence in the literature that GOES brightness temperature images of cold cloud tops show fine structures with 5–10 km spatial scale, e.g. Bedka et al. (2010),

ACPD
10, 16475–16496, 2010

finds very cold clouds just resolved with GOES and MODIS data protruding above large cold anvils. These clouds appear to be buoyant convective bubbles, referred to in the following as Protruding Convective Bubbles (PCBs), several kilometer higher than the surrounding cold anvil. With the assumption that the cold anvil reaches the tropopause, the top of a several km high PCB above the cloud top implies stratosphere penetration. The linear combination of model data shows that cloud tops well below the tropopause with an imbedded PCB can have an inverted spectrum. Assume the cloud top is at 150 hPa (approximately 210 K), i.e. about 50 hPa and 3 km below the tropopause, without a PCB. This is seen by AIRS as bt1231=210 K and DT=0 K. Assume a 5 km diameter imbedded PCB, with the same composition as the anvil, reaches the tropopause. With a 5 km FOV this would be detected as a DT=−10 K inverted spectrum. Averaged in the 15 km AIRS FOV it would appear as a bt1231=201.5 K cloud, with a DT=−1 K. If the PCB were to penetrate several km into the stratosphere, it would have to cross the level of neutral buoyancy (LNB) and the spectral inversion decreases. For the DT< −4 K conditions the entire anvil has to reach 200 K or several imbedded PCBs are required. We conclude that AIRS data are consistent with PCBs that reach the tropopause, and what is referred to as OC appear to be PCBs.

A model where the AIRS 15 km FOV includes one or more PCBs which reach or cross the LNB helps to explain what appears to be an inconsistencies related to the rain rate associated with DCC: The rain rate under DCC conditions is a factor of 40 higher than under average conditions and Fig. 4 shows the rapid increase in the rain rate with DT−2 K, but even there the average 4 mm/hr rain rate is not particularly high. The association between cold cloud tops and rain rate in the form of the GOES Precipitation Index (e.g. Arkin, 1979) is based on the 5 km GOES FOV. In the GOES data the rain rate starts to increase steeply for cloud top temperatures colder than 230 K, but with the AIRS 15 km footprint the rain rate does not increase steeply until DT=−2 K, roughly equivalent to bt1231=205 K. This inconsistency can be explained by imbedded PCBs. If the rain rate is confined to a 5 km area associated with a BB, the 4 mm/hr average rate associated with DT< −2 K spectra would be more than a factor of 10 higher locally.

ACPD
10, 16475–16496, 2010

The rain rate should increase steeply as the PCB imbedded in the anvil is pushed to the LNB. The signal contributed by one PCB, although averaged in the AIRS 15 km FOV, causes a detectable inversion in the AIRS spectra and the steep increase in the rain rate.

4.3 DCC and storms

Various proxies have been proposed for the detection of severe storms using remote sensing from Earth orbit or geostationary positions. The association between cloud top temperatures colder than 210 K in the 11 µm GOES window channel and 5 km FOV with severe storms, including torrential rain and hail over land is relatively secure and goes back to Reynolds (1980). A number of papers (e.g. Adler et al., 1985; Brunner et al., 2007) have associated OC detected with GOES with severe storms and strong horizontal and vertical wind shear. Bedka et al. (2010) used five years of GOES-12 data and MODIS data for the Gulf Stream and the US Great Plains to show the strong relationship between OC, aviation turbulence and lightening activity. Over ocean the relationship between storms and DCC is not as clear. Liu and Zipser (2005) argued based on the relative lack of lightening activity and Precipitation Features (PF) over ocean, that high clouds identified by their low brightness temperatures in IR window channels are associated with storms much weaker than their land counterparts. Based on the correlative evidence we conclude that AIRS 15 km footprints identified as DCCi, i.e. with DT< -2 K and the likely presence of one or more PCBs, indicate the presence of an unusual and therefore likely significant storm, although it is not clear from the AIRS, AMSU and AMSRe data alone if a DCCi approaches a "severe storm" as defined by the US Weather Services. In any case, long-term trends in the statistical properties of DCCi should be interesting indicators of climate change.

ACPD
10, 16475–16496, 2010

5 Conclusions

Strong convection causes cloud tops to rise close to the tropopause. Protruding above these cloud tops, but not spatially resolved by the AIRS 15 km FOV, are convective bubbles (PCBs) which reach the tropopause. The PCBs are detected as inverted AIRS spectra. Tropopause penetration is not required. The intense convection creates cold bulges in the tropopause, which are not present in the reanalysis. This gives the appearance of clouds overshooting the tropopause and penetrating into the stratosphere. The contents of the cold bulges may be left in the lower stratosphere, when the convection supporting the bulges subsides. Footprints with spectra with more than 2 K inversion (TD< −2 K), which are found for 0.4% of the AIRS spectra in the tropical oceans, are associated with a rapid increase in the rain rate. The high rain rate and the likely presence of PCBs suggests that AIRS footprints identified with DT< −2 K are associated with significant, but not necessarily severe storms.

Acknowledgements. The research described in this paper was carried out at the Jet Propulsion Laboratory, California Institute of Technology, under a contract with the National Aeronautics and Space Administration, and at UMBC, supported by NASA HQ. We are grateful for the long-term support of Ramesh Kakar, Aqua Program Scientist at NASA HQ.

References

Ackerman, S. A.: Global satellite observations of negative brightness temperature differences between 11 and 6.7 microns, J. Atmos. Sci., 53, 2803–2812, 1996.

Adler, R. F., Markus, M. J., and Fen, D. D.: Detection of severe Midwest Thunderstorms using Geosynchronous Satellite Data, Mon. Weather Rev., 113, 769–781, 1985.

Arkin, P. A.: The relationship between the fractional coverage of high cloud and rainfall accumulations during GATE over the B-array, Mon. Weather Rev., 107, 1382–1387, 1979.

Aumann, H. H., Broberg, S., Elliott, D., Gaiser, S., and Gregorich, D.: Three years of Atmospheric Infrared Sounder radiometric calibration validation using sea surface temperatures, J. Geophys. Res., 111, D16S90, doi:10.1029/2005JD006822, 2006.

ACPD

10, 16475–16496, 2010

Aumann, H. H., Chahine, M. T., Gautier, C., Goldberg, M., Kalnay, E., McMillin, L., Revercomb, H., Rosenkranz, P. W., Smith, W. L., Staelin, D. H., Strow, L., and Susskind, J.: AIRS/AMSU/HSB on the Aqua Mission: Design, Science Objectives, Data Products and Processing System, IEEE T. Geosci. Remote, 41.2, 253–264, 2003.

Baran, A. J.: Simulation of infrared scattering from ice aggregates by use of a size-shape distribution of circular ice cylinders, Appl. Optics, 42, 2811–2818, 2003.

Bedka, K., Brunner, J., Dworak, R., Feltz, W., Otkin, J., and Greenwald, T.: Objective Satellite-based Overshooting Top Detection Using Infrared Window Channel Brightness Temperature Gradients, J. Appl. Meteorol. Clim., doi:10.1175/2009JAMC2286.1, 2010.

Brunner, J. C., Ackerman, S. A., Bachmeier, A. S., and Rabin, R. M.: A quantitative Analysis of the Enhanced-V Feature in Relation to Severe Weather, Wea. Forecast., 22, 853–872, 2007.

Chou, M. D., Lee, K. T., Tsay, S. C., and Fu, Q.: Parameterization for cloud longwave scattering for use in Atmospheric Models, J. Climate, 12, 159–169, 1999.

Elliott, D. E, Aumann, H. H., Strow, L. L., and Gregorich, D. T.: Contributions to Climate Studies from four years of hyperspectral data from the Atmospheric Infrared Satellite (AIRS), Proc. SPIE, 667, edited by: Butler, J. J. and Xiong, J., 2007.

Gettelman, A., Salby, M. L., and Sassi, F.: The distribution and influence of convection in the tropical tropopause region, J. Geophys. Res., 107, D10, doi:10.1029/2001JD001048, 2002.

Imaoka, Keiji, Kachi, Misako, Shibata, Akira, Kasahara, Marehito, Iida, Yukiei, Tange, Yoshio, Nakagawa, Keizo, Shimoda, Haruhisa: Five years of AMSR-E monitoring and successive GCOM-W1/AMSR2 instrument, Proc. SPIE, 67440J, doi:10.1117/12.740366, 2007.

Iwasaki, S., Shibata, T., Nakamoto, J., Okamoto, H., Ishimoto, H., and Kukota, H.: Characteristics of deep convection measured by the A-train constellation, J. Geophys. Res., 115, D06201, doi:10.1029/2009JD013000, 2010.

Kalnay, E. and coauthors: The NCEP/NCAR 40 year reanalysis project, B. Am. Meteorol. Soc., 77, 437–471, 1996.

Lambrigtsen, B. H.: Calibration of the AIRS Microwave Instruments, IEEE T. Geosci. Remote, 41.2, 369–378, 2003.

Lane, T. P., Sharman, R. D., Clark, T. L., and Hsu, H. M.: An investigation of turbulence generation mechanisms above deep convection, J. Atmos. Sci., 60, 1297–1321, 2003.

Liu Chuntao and Zipser, E. J.: Global distribution of convection penetrating the tropical tropopause, J. Geophys. Res., 110, D23104, doi:10.1029/2005JD006063, 2005.

ACPD
10, 16475–16496, 2010

Randel, J. W., Park, M., Emmons, L., Kinnison, D., Bernath, P., Walker, K. A., Boone, C., and Pumphrey, H.: Asian Monsoon Transport of Pollution to the Stratosphere, Science, 328, 611–613, doi:10.1126/science.1182274, 2010.

Ray, E. A. and Rosenlof, K. H.: Hydration of the upper tropopause by tropical cyclones, J. Geophys. Res., 112, D12311, doi:10.1029/2006JD008009, 2007.

Reynolds, D. W.: Observations of Damaging Hailstorms from Geosynchronous Satellite Digital Data, Mon. Weather Rev., 108, 337–348, 1980.

Romps, D. M. and Kuang, Z.: Overshooting Convection in tropical cyclones, Geophys. Res. Lett., 36, L09804, doi:10.1029/2009GL037396, 2009.

Schmetz, J., Tjemkes, S. A., Gube, M., van de Berg, L.: Monitoring deep convection and convective overshooting with METEOSAT, Adv. Space Res., 19, 3, 433–441, 1997.

Strow, L. L., Hannon, S., DeSouza-Machado, S., Tobin, D., and Motteler, H.: An overview of the AIRS Radiative Transfer Model, IEEE T. Geosci. Remote, 41, 303–313, 2003.

TIGR3: A large collection of RAOBs available from Laboratoire de Meteorologie Dynamique (LMD), France, 1999.

Walden, V. P., Roth, W. L., Stone, R. S., and Halter, B.: Radiometric Validation of the AIRS Infrared Sounder over the Antarctic Plateau, J. Geophys. Res., 111, doi:10.1029/2005JD006357, 2006.

Wang, P.: The thermodynamic structure atop a penetrating convective thunderstorm, Atmos. Res., 83, 254–262, 2007.

Wilheit, T., Kummerow, C. D., and Ferraro, R.: Rainfall Algorithms for AMSRE, IEEE T. Geosci. Remote, 41.2, 204–214, 2003.

Zelinka, M. and Hartmann, D. L.: Response of Humidity and Clouds to Tropical Deep Convection, J. Climate, 22, 2389–2404, doi:10.1175/2008JCLI2452.1, 2009.

ACPD
10, 16475–16496, 2010

Table 1. Summary of the frequency distribution of cold clouds with the 15 km AIRS FOV.

	Day TO frequency [%]	Night TO frequency [%]	Day WTP frequency [%]	Night WTP frequency [%]
bt1231<260 K	9.78	8.37	16.62	17.3
bt1231<250 K	7.43	5.93	13.12	12.78
bt1231<235K	4.77	3.80	9.23	8.74
bt1231<225 K	3.34	2.84	6.67	6.96
bt1231<215 K	1.31	1.44	3.32	3.58
bt1231<210 K	0.39	0.69	1.97	2.41
bt1231-bt1419<0 K	0.72	0.92	1.87	2.23
bt1231-bt1419< −2 K	0.36	0.54	1.02	1.31
bt1231-bt1419< −4 K	0.11	0.26	0.36	0.52
bt1231-bt1419< −6 K	0.02	0.06	0.10	0.17
bt1231-bt712<0 K	0.63	0.87	1.45	2.13
bt1231-bt712< −2 K	0.32	0.52	0.86	1.31
bt1231-bt712< −4 K	0.10	0.27	0.27	0.54
bt1231-bt712< −6 K	0.02	0.08	0.09	0.21

ACPD
10, 16475–16496, 2010

Table 2. Summary of results for DCC under random and DT< −2 conditions for 7 years of data.

	Day TO	Night TO	Day WTP	Night WTP
AMSU#14 mean [K]	252.76	251.75	252.98	252.55
DT< −2 K condition	253.43	253.43	252.93	253.37
(DT< −2 K)-mean	+0.3	+1.7	−0	+0.78
AMSU#9 mean [K]	205.19	206.57	205.47	206.57
(DT< −2 K) condition	205.06	204.16	205.35	204.16
(DT< −2 K)-mean	−0.13	−2.4	−0.12	−2.5
AIRS 668.2 3 hPa mean	246.64	246.52	246.22	245.70
(DT< −2 K) conditions	246.83	247.35	246.98	247.09
(DT<-2 K)-mean	+0.2	+0.8	+0.8	+1.4
AIRS 679.2 40 hPa mean	211.81	212.58	212.00	212.25
(DT< −2 K) conditions	211.72	210.80	211.82	210.65
(DT< −2 K)-mean	−0.1	−1.8	−0.2	−1.6
3–40 hPA amplitude K	0.3	2.6	1.0	3.0
Rain rate				
(DT< −2 K) condition mean [mm/hr]	3.94	5.73	3.21	3.82
Random condition mean [mm/hr]	0.12	0.13	0.20	0.25
bt1231 1% tile/99% tile [K] (DT< −2 K)	190–208	188–207	190–207	190–208
(bt961-bt790) [K]				
Mean DT=0 K	1.20	1.11	1.29	1.24
Mean DT< −2 K	1.08	0.97	1.12	1.11
Mean DT< −4 K	0.98	0.82	0.86	0.99
Mean DT< −6 K	0.84	0.82	0.76	0.73
Stdev K	0.67	0.63	0.70	0.67

ACPD
10, 16475–16496, 2010

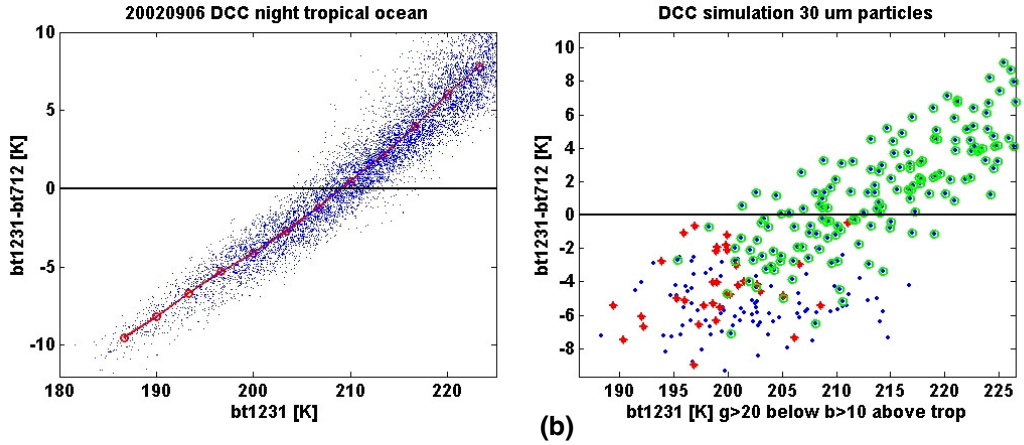

Fig. 1. bt1231-bt712 (DT) vs bt1231 for spectra with bt1231<225 K, **(a)** shows the observations from one day (6 September 2002, 1:30 a.m. overpasses), **(b)** shows the results of the DCC simulations: blue (x) = more than 5 hPa above, red (+) = within 5 hPa of, and green (o) = more than 5 hPa below the tropopause of the model atmosphere. Since the profiles used for the model runs match the mean, but not the dispersion of real tropical spectra, the model results appear to be more dispersed.

ACPD
10, 16475–16496, 2010

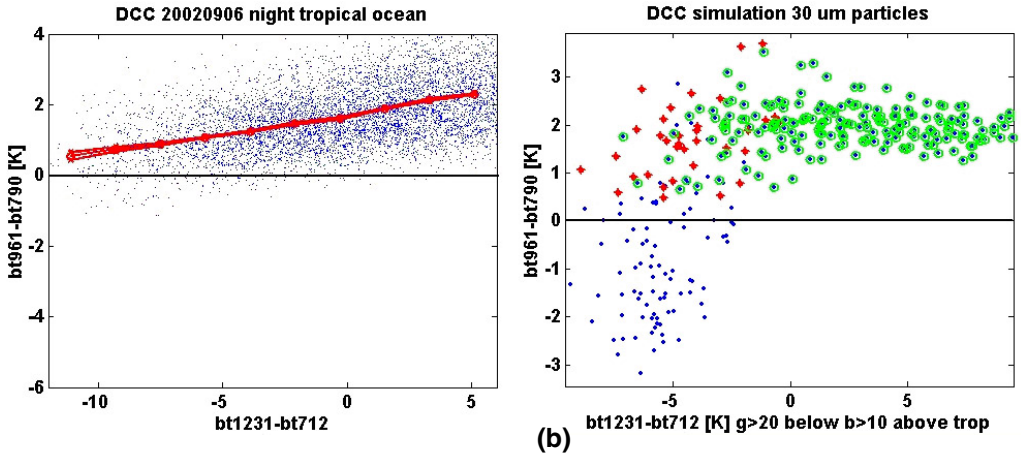

Fig. 2. bt961-bt790 (DC) vs. bt1231-bt712 (DT) for spectra with bt1231<225 K, **(a)** from the same data used in Fig. 1a, **(b)** model results on the same scale.

ACPD
10, 16475–16496, 2010

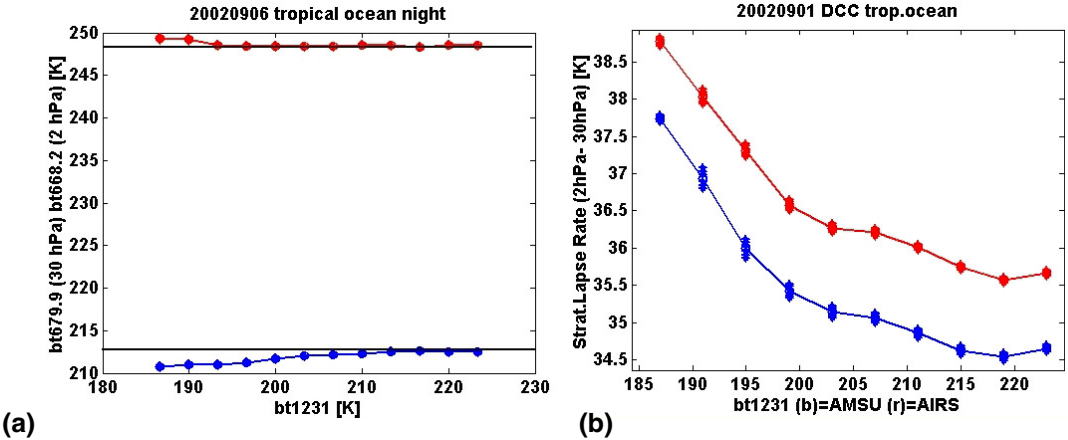

Fig. 3. Scatter diagram of temperatures above the tropopause as function of bt1231. **(a)** 2 hPa (red) and 40 hPa (blue) using AIRS channels. **(b)** Lapse rate using approximately equivalent AMSU (blue) and AIRS (red) channels.

ACPD
10, 16475–16496, 2010

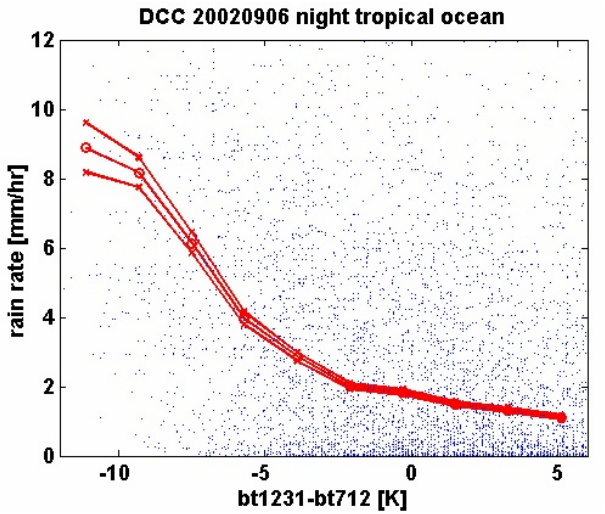

Fig. 4. Rain rate as function of DT. The three lines represent the ridge line ± its probable error. (maybe red line with ± black lines?)

ACPD
10, 16475–16496, 2010